Received: 3 March 2022 | Revised: 23 July 2022 | Accepted: 13 August 2022

DOI: 10.1002/jev2.12261

RESEARCH ARTICLE

Necroptosis is associated with Rab27-independent expulsion of extracellular vesicles containing RIPK3 and MLKL

Kartik Gupta[1] | **Kyle A. Brown**[1,2] | **Marvin L. Hsieh**[1] | **Brandon M. Hoover**[5] | **Jianxin Wang**[6] | **Mitri K. Khoury**[1] | **Vijaya Satish Sekhar Pilli**[1] | **Reagan S. H. Beyer**[1] | **Nihal R. Voruganti**[1] | **Sahil Chaudhary**[1] | **David S. Roberts**[2] | **Regina M. Murphy**[5] | **Seungpyo Hong**[6,7] | **Ying Ge**[2,3,4] | **Bo Liu**[1,3]

[1]Division of Vascular Surgery, Department of Surgery, University of Wisconsin-Madison, Madison, Wisconsin 53705, USA

[2]Department of Chemistry, University of Wisconsin-Madison, Madison, Wisconsin 53705, USA

[3]Department of Cell and Regenerative Biology, University of Wisconsin-Madison, Madison, Wisconsin 53705, USA

[4]Human Proteomics Program, School of Medicine and Public Health, University of Wisconsin-Madison, Madison, Wisconsin 53705, USA

[5]Department of Chemical and Biological Engineering, University of Wisconsin-Madison, Madison, Wisconsin 53705, USA

[6]Wisconsin Center for NanoBioSystems, School of Pharmacy, University of Wisconsin-Madison, Madison, Wisconsin 53705, USA

[7]Pharmaceutical Sciences Division, School of Pharmacy, University of Wisconsin-Madison, Madison, Wisconsin 53705, USA

Correspondence
Bo Liu, PhD, Division of Vascular Surgery, Department of Surgery, University of Wisconsin-Madison, 1111 Highland Avenue, Madison, WI 53705, USA.
Email: liub@surgery.wisc.edu

Current address of Kartik Gupta Weatherwax Biotechnologies, 953 Indiana Street, San Francisco CA 94107, USA.

Lead Contact: Bo Liu.

Abstract

Extracellular vesicle (EV) secretion is an important mechanism used by cells to release biomolecules. A common necroptosis effector—mixed lineage kinase domain like (MLKL)—was recently found to participate in the biogenesis of small and large EVs independent of its function in necroptosis. The objective of the current study is to gain mechanistic insights into EV biogenesis during necroptosis. Assessing EV number by nanoparticle tracking analysis revealed an increased number of EVs released during necroptosis. To evaluate the nature of such vesicles, we performed a newly adapted, highly sensitive mass spectrometry-based proteomics on EVs released by healthy or necroptotic cells. Compared to EVs released by healthy cells, EVs released during necroptosis contained a markedly higher number of unique proteins. Receptor interacting protein kinase-3 (RIPK3) and MLKL were among the proteins enriched in EVs released during necroptosis. Further, mouse embryonic fibroblasts (MEFs) derived from mice deficient of Rab27a and Rab27b showed diminished basal EV release but responded to necroptosis with enhanced EV biogenesis as the wildtype MEFs. In contrast, necroptosis-associated EVs were sensitive to Ca^{2+} depletion or lysosomal disruption. Neither treatment affected the RIPK3-mediated MLKL phosphorylation. An unbiased screen using RIPK3 immunoprecipitation-mass spectrometry on necroptotic EVs led to the identification of Rab11b in RIPK3 immune-complexes. Our data suggests that necroptosis switches EV biogenesis from a Rab27a/b dependent mechanism to a lysosomal mediated mechanism.

KEYWORDS
lysosomal exocytosis, MLKL, necroptosis, proteomics, RIPK3, SEVs

Kartik Gupta and Kyle A. Brown contributed equally to this study.

1 | INTRODUCTION

The receptor-interacting protein kinase (RIP) family members RIPK1 and RIPK3 play a crucial role in the initiation of a form of regulated necrosis called necroptosis (Cho et al., 2009; He et al., 2009). The association of RIPK3 with RIPK1 via RHIM-domain interaction and subsequent trans-autophosphorylation events lead to RIPK3 activation (Sun et al., 2002). Activated RIPK3 interacts with and phosphorylates a pseudokinase called mixed lineage kinase domain-like (MLKL). The translocation of MLKL to the plasma membrane is required for the rupture of the plasma membrane during necroptosis (Cai et al., 2014; Hildebrand et al., 2014; Su et al., 2014). The dynamic process of exocytosis and endocytosis, by repairing the damaged plasma membrane, can alter the threshold at which cells become terminally necrotic (Fan et al., 2019; Gong et al., 2017; Yoon et al., 2017; Zargarian et al., 2017). Loss of MLKL can completely rescue necrosis even upon sustained activation of upstream signalling via RIPK1-RIPK3 by preventing lysis of the plasma membrane (Wu et al., 2013). The delay in the lysis of the plasma membrane during necroptosis is likely to minimize the release of various intracellular molecules that can serve as damage-associated molecular patterns (DAMPs) and cause an inflammatory response (Rock & Kono, 2008).

Extracellular vesicles (EVs) are membrane-bound, micron to submicron-sized vesicles that are released from cells. EVs are increasingly recognized as a mechanism of cell-cell communication in health and disease. A subset of these vesicles, called small EVs (SEVs), encompass 30–200 nm sized vesicles (Harmati et al., 2019; Walbrecq et al., 2020) some of which are produced via the endocytic machinery. Additionally, when these SEVs contain key cargo reflective of ongoing cellular events and are produced via the ESCRT pathway, these may be referred to as exosomes. The Rab family of proteins regulates many steps that are essential in vesicular trafficking such as formation, motility and fusion (Grosshans et al., 2006; Rink et al., 2005; Søgaard et al., 1994). These monomeric GTPase proteins shuttle between a GTP-bound active and GDP-bound inactive state. Specifically, Rab27a and Rab27b are widely known to promote distinct steps of SEV release from cells (Fukuda, 2013; Ostrowski et al., 2010). New evidence also suggests that other routes of SEV exocytosis may co-exist with Rab27-mediated exocytosis (Tanzer et al., 2020). Other Rab proteins are essential for the upstream steps of SEV biogenesis. Towards this, the Rab11 family of proteins including Rab11a, Rab11b and Rab25 regulates several steps of MVB formation through recycling endosomes (Savina et al., 2005; Willoughby et al., 2021), a subset of which are essential for SEV formation. Curiously, the Rab11 family is found to be enriched in SEVs (Shlomovitz et al., 2021) and has also been identified to interact with RIPK3 during necroptosis (Zhang et al., 2009).

Recent work has shown that dying cells may generate SEVs that expel proteins with cell-harming properties (Tanzer et al., 2020). Therefore, EV release may, on one hand, protect the host cells, but on the other hand, may impose a danger to other cells. In this regard, necroptotic cell death is intriguing as cells not only generate SEVs during necroptosis but the effector protein MLKL is fundamental to the biogenesis of SEVs even in healthy cells (Tanzer et al., 2020; Yoon et al., 2017). Several groups have independently demonstrated the role of MLKL in the endocytotic and exocytotic mode of SEV biogenesis via the ESCRT complex (Gong et al., 2017; Yoon et al., 2017). In both these processes, RIPK3-mediated MLKL phosphorylation enhances SEV biogenesis.

Interestingly, phosphorylation of MLKL by RIPK3 also results in its translocation to the plasma membrane and the subsequent influx of calcium from the extracellular environment (Cai et al., 2014). However, the phosphorylation of MLKL is a non-committal step in necroptosis as various "checkpoints" exist to ensure adequate opportunities for cells to repair membrane damage before necrosis (Samson et al., 2020). The influx of calcium from damaged plasma membrane may facilitate plasma membrane repair through a process called lysosomal exocytosis (Reddy et al., 2001). During lysosomal exocytosis, the fusion of the lysosomal membrane—a calcium-dependent process—prevents further damage to the plasma membrane (Jaiswal et al., 2002). Paradoxically, MLKL appears to facilitate plasma membrane repair via calcium influx but is immediately cleared out from cells through extrusion in SEVs or by internalization in lysosomes followed by its degradation (Fan et al., 2019). Despite the key role of RIPK3 in phosphorylating MLKL, its involvement in the process of SEV biogenesis remains unknown.

In this report, we profile the protein contents of SEVs released by healthy and necroptotic cells using high-sensitivity mass spectrometry (MS)-based proteomics enabled by a photocleavable surfactant (Aballo et al., 2021; Brown et al., 2019, 2020b) and Bruker timsTOF Pro Q-TOF (Meier et al., 2018). We identify that the necroptotic mediators RIPK3 and MLKL are enriched inside SEVs released by necroptotic cells. Further, we provide mechanistic insights on how cells respond to necroptotic insults by adopting a lysosomal route of vesicle release to expel RIPK3 and MLKL.

2 | MATERIAL AND METHODS

2.1 | Cell culture

Mouse embryonic fibroblasts (MEFs) were isolated from E12.5 littermate *Ripk3*$^{+/+}$ or *Ripk3*$^{-/-}$ mice. HT29 cells were obtained from American Type Culture Centre. All cells were cultured in DMEM medium (4.5 g/L glucose) under 10% FBS and 1% penicillin-streptomycin in a humidified chamber at 37°C under 5% CO_2. Media was changed every 2–3 days and cells were passaged using 0.05% trypsin. EV-depleted FBS (System Biosciences) was used for cells whose SEVs were used in experiments.

2.2 | Cell-death induction

For the induction of necroptosis, MEFs were pre-treated with 10 μM BV6 (Smac mimetic) and 20 μM zVAD-fmk (hereafter zVAD) for 1 h. Recombinant mouse TNFα (50 ng/ml, R&D systems) was added for 6 h unless stated otherwise. HT29 cells were pre-treated with 10 μM BV6 and/or 20 μM zVAD for 1 h. Recombinant human TNFα (30 ng/ml) was added for 4 h. Cell-death was evaluated using Annexin V/7-AAD (BD Biosciences) coupled with flow-cytometry.

2.3 | EV isolation from cells

Differential centrifugation was used for SEV isolation unless otherwise specified. Briefly, conditioned media or plasma were spun at 800 g for 10 min to remove cells and large cell debris. The supernatant was transferred and spun at 10,000 × *g* for 30 min at 4°C. The supernatant was carefully harvested and centrifugation was performed at 100,000 × *g* at 4°C for 90 min. The supernatant was discarded and the pellet was dissolved in PBS. SEVs were also isolated using ExoQuick-TC (System BioSciences) as per the manufacturer's instructions. For selected experiments, size exclusion chromatography, qEVoriginal/35 nm Gen 2 Column (IZON Science LTD, MA) was used, per manufacturer's instructions, as an extra purification step following ultracentrifugation. Briefly, conditioned media was pre-cleared using step-wise centrifugation described above. An enrichment of SEVs (along with any putative protein contaminants) was performed using ultracentrifugation and resuspension in 500 μl of PBS. Next, to separate any putative protein contaminants from SEVs, size exclusion chromatography was performed (Veerman et al., 2021). The fraction corresponding to SEVs (expected to be separated from protein contaminants) was collected in 1.5 ml PBS. Because the concentration of SEVs collected after SEC was low, a concentrating step (via ultracentrifugation) was added and SEVs were resuspended in a final volume of 100 μl.

2.4 | EV isolation from human and mouse plasma

Mouse blood was collected from 8 to 12-week-old mice via inferior vena cava (IVC) puncture and supplemented with 3.2% sodium citrate as an anticoagulant (9:1). Blood samples were centrifuged at 1000 × *g* for 10 min at 4°C. The supernatant was collected and spun at 10,000 × *g* for 20 min at 4°C to remove residual platelets. SEVs were isolated from human and mouse plasma using ExoQuick Ultra (System Biosciences) according to manufacturer's instructions. Prior to SEV isolation from plasma, plasma samples were treated with PureProteome Albumin/IgG Depletion kit (Millipore Sigma, LSKMAGD12) according to manufacturer's instructions. Differential centrifugation was also used for SEV isolation. Briefly, plasma was spun at 10,000 × *g* for 1 h at 4°C. The supernatant was carefully harvested and centrifugation was performed at 100,000 × *g* at 4°C for 90 min. The supernatant was discarded and the pellet was dissolved in PBS.

2.5 | Nanoparticle tracking analysis (NTA)

The size distribution and particle concentration of the isolated EVs were measured using a Nanosight NS300 equipped with Nanosight NTA 3.3 software and a 532 nm laser (Malvern Instruments, UK). Three videos at 60 s each were recorded for all EV samples at camera level 15 and syringe pump speed of 70 units. The analysis was done at 25 frames/s with a detection threshold of four. All samples were diluted to the appropriate concentration in PBS prior to measurement.

2.6 | Mass spectrometry

Purified exosomes in 225 μl of 25 mM ammonium bicarbonate (ABC) pH seven were lysed with 25 μl of the solubilization buffer consisting of 0.5% 4-hexylphenylazosulfonate (final surfactant concentration, 0.05%) (Brown et al., 2019, 2020a). Samples were then reduced using 4 μl of 100 mM tris(2-carboxyethyl)phosphine (TCEP) and alkylated with 4 μl of 500 mM 2-chloroacetamide solution and incubated at room temperature for 30 min. Proteins were digested using 2 μl of 0.3 μg/μl Trypsin solution and incubated at 37°C for 1 h. The surfactant was degraded with 5 min of UV using a 100 W mercury lamp (Nikon housing with Nikon HB-10101AF power supply; handle with caution). 2 μl of TFA (10%) was added to samples, which were then vortexed and centrifuged at 20,000 × *g* for 2 min. Using a ZipTip (Pierce™ C18 Tips, 100 μl bed), the samples were desalted according to the manufacturer's instructions. The samples were reconstituted in 25 μl of mobile phase solvent A (99.8% water and 0.2% formic acid). The peptide concentration was determined using NanoDrop operating at 280 nm.

Approximately 200 ng of peptide were loaded onto an Ion Optics column (25 cm × 75 μm, C18 1.6 μm) heated to 55°C. The separation was performed using the following gradient: 0–60 min 2%–17% B, 60–90 min 17%–25% B, 90–100 min 37% B, 100–110 min 37%–85% B, and 110–120 min 85% B using a flow rate of 400 nl/min and mobile phase B consisting of 99.8% ACN and 0.2% formic acid. Eluting peptides were directly ionized via electrospray ionization (CaptiveSpray) using a capillary voltage of 1500 V, dry gas of 3.0 L/min, and dry temp of 180°C. Ions measured from 100 to 1700 *m/z* using a timsTOF Pro Q-TOF (Bruker Daltonics) operating in PASEF mode (Meier et al., 2018) with an ion mobility range (1/k0) of 0.60–1.60 Vs/cm^2. For tandem MS, the following parameters were used: number of PASEF MS/MS scans (10); total cycle time (1.16 s); target intensity (20000); intensity threshold (2500); charge range (0–5); isolation width (2 *m/z* for $m/z < 700$ and 3 *m/z* for $m/z > 700$); collisional energy (20–59 eV). Precursor ions were excluded within a 0.4 min widow and reconsidered if the intensity was 4-fold of the previous selection. The performance of the instrument (as well as validation of the peptide loading amount) was monitored periodically by running 200 ng of standard K652 digestion (Promega). Data were processed using MSFragger V15.0 software (Yu et al., 2020). For database searches, we used the reviewed Mus musculus (Mouse) UniProt sequences (https://www.uniprot.org, October 7, 2020) using a 1% false discovery rate. All searches were performed with carbamidomethyl (C) as a fixed modification and oxidation (M), protein N-terminal acetylation, and phosphorylation (STY) set as variable modifications. Match between runs was enabled. Otherwise, the MSFragger parameters were not changed from their default values.

For the IP analysis, samples were precipitated in 500 μl acetone overnight. After centrifugation (20,000 × *g*, 10 min, 4°C), 30 μl of ABC was added to each along with 10 mM TCEP, 20 mM 2-chloroacetamide, and 1 μg trypsin. Samples were digested overnight at 4°C. 2 μl of TFA (10%) was added to quench the digestion. Data were processed using MSFragger V15.0 as described above. The data were deposited to the ProteomeXchange Consortium via the PRIDE (Perez-Riverol et al., 2019) partner repository with the dataset identifier PXD031224.

2.7 | Electron microscopy (EM)

Isolated SEVs were fixed with 2% paraformaldehyde, adhered to a carbon-grid for 20 mins, and analyzed by transmission EM after eight washes and embedded in 2% methylcellulose with 0.4% uranyl acetate.

2.8 | Proteinase-K digestion of SEVs

EVs isolated from MEFs treated with TNFα, Smac-mimetic, and zVAD (TSZ) via ExoQuick were resuspended in Dulbecco's phosphate-buffered saline. The mix was incubated at 37°C with or without Triton X-100(1% v/v) where indicated. For proteinase K digestion, SEVs were treated with 10^{-5} units/ml proteinase K (New England BioLabs, Cat#:P8107S), Triton X-100(1% v/v), and 15 mm $CaCl_2$. The presence of RIPK3 was then detected via Western blotting.

2.9 | Flow cytometry

Annexin V-PE and 7-AAD staining Kit (BD Biosciences, San Jose, CA) kit was used for cell-death analysis. Cells were rinsed with Dulbecco's phosphate-buffered saline and incubated with 0.25% trypsin at 37°C for 2 min. All cells (from culture medium, PBS wash, and trypsin treatment) were collected by centrifugation (2000 × *g*, 5 min). Cell pellets were further washed with PBS and resuspended in 1 ml of binding buffer from the Annexin V-PE/7-AAD staining Kit. 5 μl of PE Annexin-V and 5 μl of 7-AAD were added to the cells and incubated at room temperature for 15 min. 400 μl binding buffer was added to each sample after incubation. Cells were analyzed using a Becton Dickinson Biosciences FACS Caliber (BD Biosciences, San Jose, CA). The population is represented as percent of Annexin V-PE$^+$ and 7-AAD$^+$ cells (Annexin V$^+$/7-AAD$^+$).

2.10 | Western blotting

Samples were loaded onto a 10% SDS-PAGE gel and then transferred to a polyvinylidene fluoride membrane. Binding of the primary antibody was detected by peroxidase-conjugated secondary antibodies and enhanced chemiluminescence. The sources of antibodies and dilutions used for Western blot analysis were as follows: anti-RIPK3(1:1000, ProSci, Cat #:2283), anti-RIPK3(1:1000, Cell Signaling Technology, Cat#:13526), anti-MLKL (1:1000, EMD Millipore, Cat#MABC604), anti-RIPK1(1:500, BD Biosciences, Cat#:610458), anti-CD63(1:1000, System Biosciences, Cat#:EXOAB-CD63A-1), anti-TSG101(1:1000, Abcam, Cat#:ab30871), anti-CD81(1:1000, System Biosciences, Cat#:EXOAB-CD81A-1), anti-CD9(1:1000, System Biosciences, EXOAB-CD9A-1), anti-Calnexin (1:1000, Cell Signalling Technology, Cat#:2433S).

2.11 | Statistical analysis

Categorical variables were represented as numbers with proportions. Continuous variables were represented as means with standard deviations (SDs) when normally distributed and medians with interquartile ranges for non-normally distributed data. Two-way ANOVA and Kruskal-Wallis ANOVA on rank were used to compare multiple groups for parametric and nonparametric data, respectively. All statistical analysis was performed using GraphPad Prism v6.0. $p < 0.05$ was considered statistically significant.

3 | RESULTS

3.1 | Necroptotic cells show enhanced activities in producing EVs

MEFs derived from *Ripk3*$^{+/+}$ or *Ripk3*$^{-/-}$ mice were subjected to necroptosis induction with TNFα in the presence of Smac-mimetic and zVAD (hereater referred to as TSZ). As expected, TSZ caused significant necrosis in *Ripk3*$^{+/+}$ MEFs but not in *Ripk3*$^{-/-}$ MEFs (Figure 1a). Next, we isolated SEVs from the conditioned media using two commonly used methods—ultracentrifugation and ExoQuick (Figure 1b). The isolated vesicles were subjected to NTA to simultaneously measure the size and concentration of the isolated vesicles (Figure 1c,d). The EVs from healthy and necroptotic cells fit the size characteristics of small EVs regardless of genotypes or isolation methods used (Figure 1e,f) and are hereby referred to as SEVs. Compared to the DMSO control, TSZ produced a dramatic increase in SEV numbers released by *Ripk3*$^{+/+}$ MEFs, an induction that was absent in *Ripk3*$^{-/-}$ MEFs (Figure 1g,h). Since both isolation methods produce identical results, we utilized ultracentrifugation-based isolation for subsequent assays.

3.2 | Proteomic analysis of necrotic SEVs reveals known and novel protein cargos

Whether necroptosis alters protein cargos in SEVs is unknown. We utilized MS-based proteomics to assess the protein cargos inside SEVs released from healthy or necroptotic cells (Figure 2a). We found SEVs released by necroptotic cells contained more varieties of proteins than those released by healthy cells: 1318 unique protein identifications in the necroptotic SEVs, 14 unique proteins in the healthy SEV, and 906 shared proteins in both healthy and necroptotic SEVs (Figure 2b, Table S1). Next, we performed various gene ontology (GO) enrichment analyses (Raudvere et al., 2019) on the proteins uniquely found in the SEVs released from necrotic cells (Figure 2c). Notably, the proteins inside SEVs had a wide array of molecular functions; the processes of vesicle-mediated transport, endocytosis, cellular localization and others were reproducibly enriched. Proteins specifically enriched in the necrotic SEVs were involved in biological processes such as intracellular transportation and cellular localization (Figure 2d). The necroptotic SEV-specific proteins were generally located in the cytosol, cytoplasm, intracellular anatomical structure, organelle, or vesicles, and analysis of their reactome indicated involvement with the metabolism of RNA, membrane trafficking, and vesicle-mediated transportation. Overall, the GO enrichment analysis provided further evidence of the successful isolation and proteomic analysis of proteins belonging to SEVs which enabled the identification of the unique cargo belonging to necroptosis SEVs.

We also compared the protein cargo identified in our proteomic analysis with the top markers for SEV cargo available in ExoCarta (Keerthikumar et al., 2016) and Vesiclepedia (Pathan et al., 2019). We identified 65 SEV proteins common among these and necrotic SEVs (Figure 2e), providing an internal validation for our isolation technique. Figure 2f lists the top protein cargos uniquely residing in SEVs released from TSZ-treated and DMSO-treated MEFs. Recently, Shlomovitz et al. performed similar proteomic experiment in U937 cell lines to which we compared the proteins identified in the study with those detected in this study. About half (1023) of the proteins identified in our mass-spectrometry experiments are shared between the two studies (Figure S1). Several cell death proteins including RIPK3 and MLKL are among the proteins that were enriched in SEVs released by necroptotic cells. STRING analysis showed that cargo proteins in necroptosis-associated SEVs are clusters in cell death pathways and protein secretion pathways, among others (Figure 2g, Table S1). Because of their unique cargo profile, we will refer to the SEVs secreted under necroptosis condition as necroptosis enhanced SEVs (NEEs) for the rest of the study.

3.3 | RIPK3 is a luminal cargo protein in NEEs

We further characterized the protein cargos associated with SEVs using Western blotting. Whole-cell lysate (WCL) and SEVs were prepared from *Ripk3*$^{+/+}$ or *Ripk3*$^{-/-}$ MEFs following treatment with DMSO or TSZ. In agreement with the proteomics data, RIPK3 was more abundant in NEEs than what was detected in SEVs from DMSO-treated *Ripk3*$^{+/+}$ MEFs (Figure 3a). A

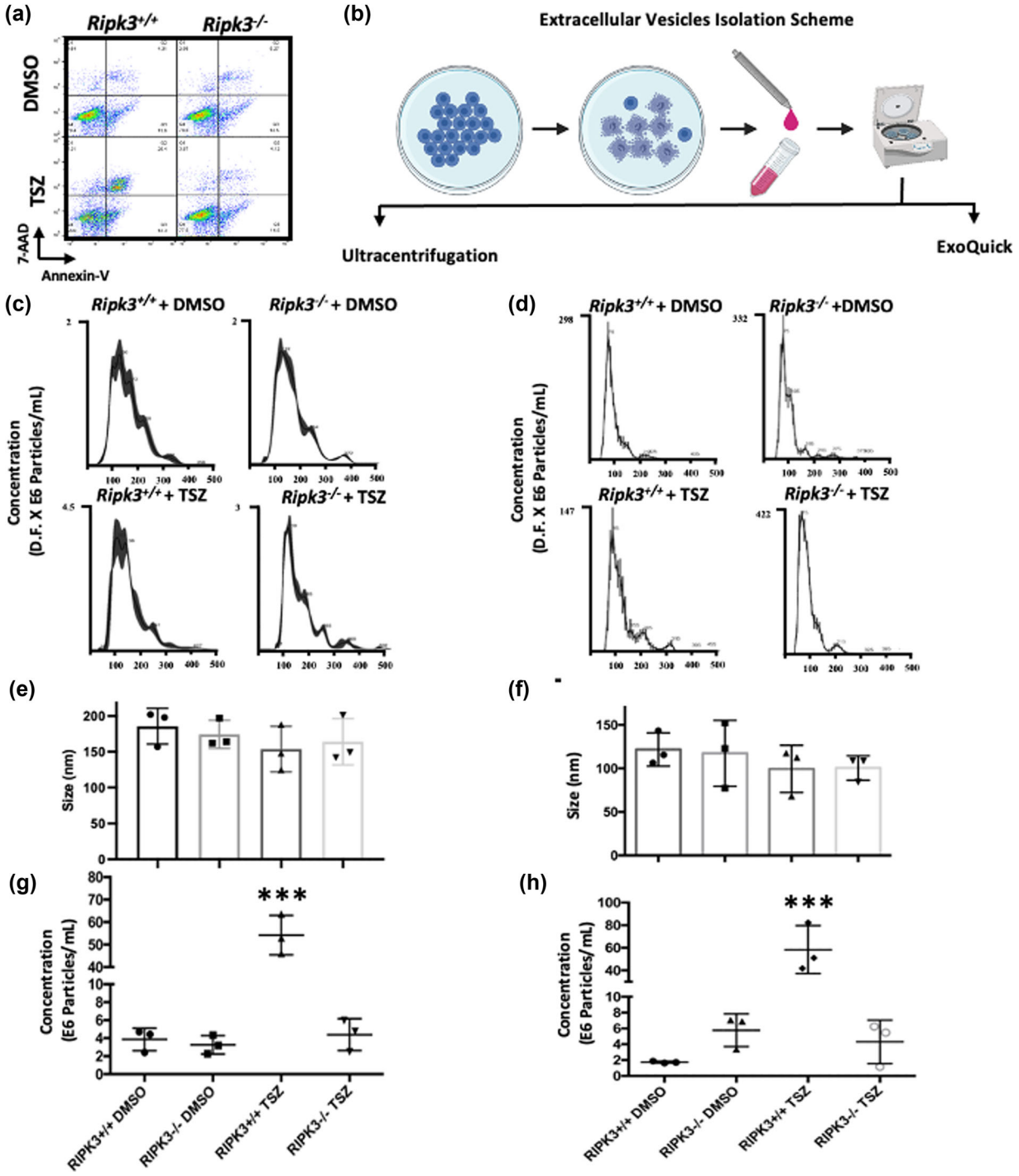

FIGURE 1 **Necroptotic cells release extracellular vesicles.** (a) *Ripk3*$^{+/+}$ and *Ripk3*$^{-/-}$ MEFs were treated with DMSO or TSZ for 6 h. Cell death was analyzed by flow cytometry. Representative scatter plot is depicted. (b) Schematic outline of SEV isolation. Cell culture media from cultured MEFs was centrifuged to remove large cellular debris and SEVs were then isolated using ultracentrifugation or ExoQuick reagent. (c and d) Representative traces from nanoparticle tracking analysis (NTA) are presented. SEVs isolated from DMSO- or TSZ-treated *Ripk3*$^{+/+}$ or *Ripk3*$^{-/-}$ MEFs were isolated by ultracentrifugation (c) or ExoQuick (d) and analyzed by NTA. (e and f) Mean particle size obtained by NTA analyses is depicted for SEVs isolated from DMSO- or TSZ-treated *Ripk3*$^{+/+}$ or *Ripk3*$^{-/-}$ MEFs by ultracentrifugation (e) or ExoQuick (f). (g and h) Mean particle number measured by NTA analysis is depicted for SEVs isolated from DMSO- or TSZ-treated *Ripk3*$^{+/+}$ or *Ripk3*$^{-/-}$ MEFs by ultracentrifugation (g) or ExoQuick (h). All data shown are mean ± SD of three or more independent experiments. ***$p < 0.001$ using one-way ANOVA (g, h)

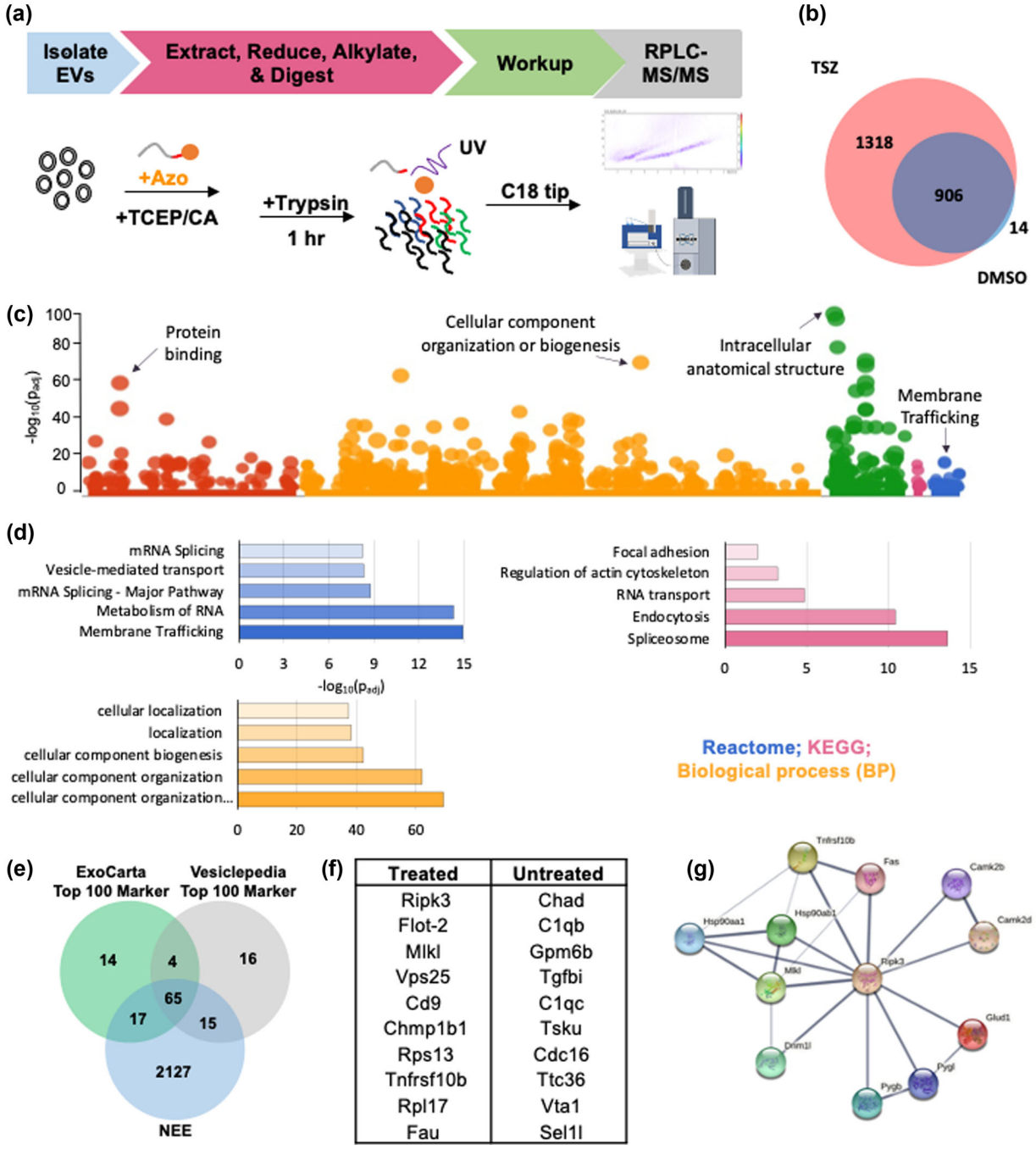

Treated	Untreated
Ripk3	Chad
Flot-2	C1qb
Mlkl	Gpm6b
Vps25	Tgfbi
Cd9	C1qc
Chmp1b1	Tsku
Rps13	Cdc16
Tnfrsf10b	Ttc36
Rpl17	Vta1
Fau	Sel1l

FIGURE 2 **Mass spectrometry (MS) analysis of NEEs.** (a) Schematic representation of MS-based proteomics workflow for the analysis of extracellular vesicles. Proteins were extracted from isolated vesicles using a photocleavable surfactant, Azo, reduced with tris(2-carboxyethyl)phosphine (TCEP), alkylated with 2-chloroacetamide (CA), digested with trypsin, and analyzed by using reversed-phase liquid chromatography-mass spectrometry (RPLC-MS) after surfactant removal. (b) Venn diagram comparing protein identified in the control (DMSO) and TSZ treated samples. (c and d) Overview of GO enrichment analysis of proteins uniquely found in the TSZ treated sample sorted by molecular function (MF), biological process, cellular component, KEGG, and reactome. (e) Comparison of proteins identified in this study with the top 100 proteins available in the ExoCarta and Vesiclepedia databases. (f) Representative proteins uniquely found in TSZ and the control samples. (g) String analysis of proteins found to interact with RIPK3

time-course study suggests that the packaging of RIPK3 in SEVs is time-dependent. A substantial fraction of RIPK3 was found in SEVs released by cells that had been treated with TSZ for 5 h or longer (Figure S2A). Since necroptosis is associated with a large-scale release of biomolecules, we performed a size exclusion-based method to further separate EVs from potential proteins released directly from ruptured cell membrane (steps outlined in Figure S2B). Western blot analysis of the SEV fractions that contained EVs confirmed the presence of RIPK3 (Figure 3b,c).

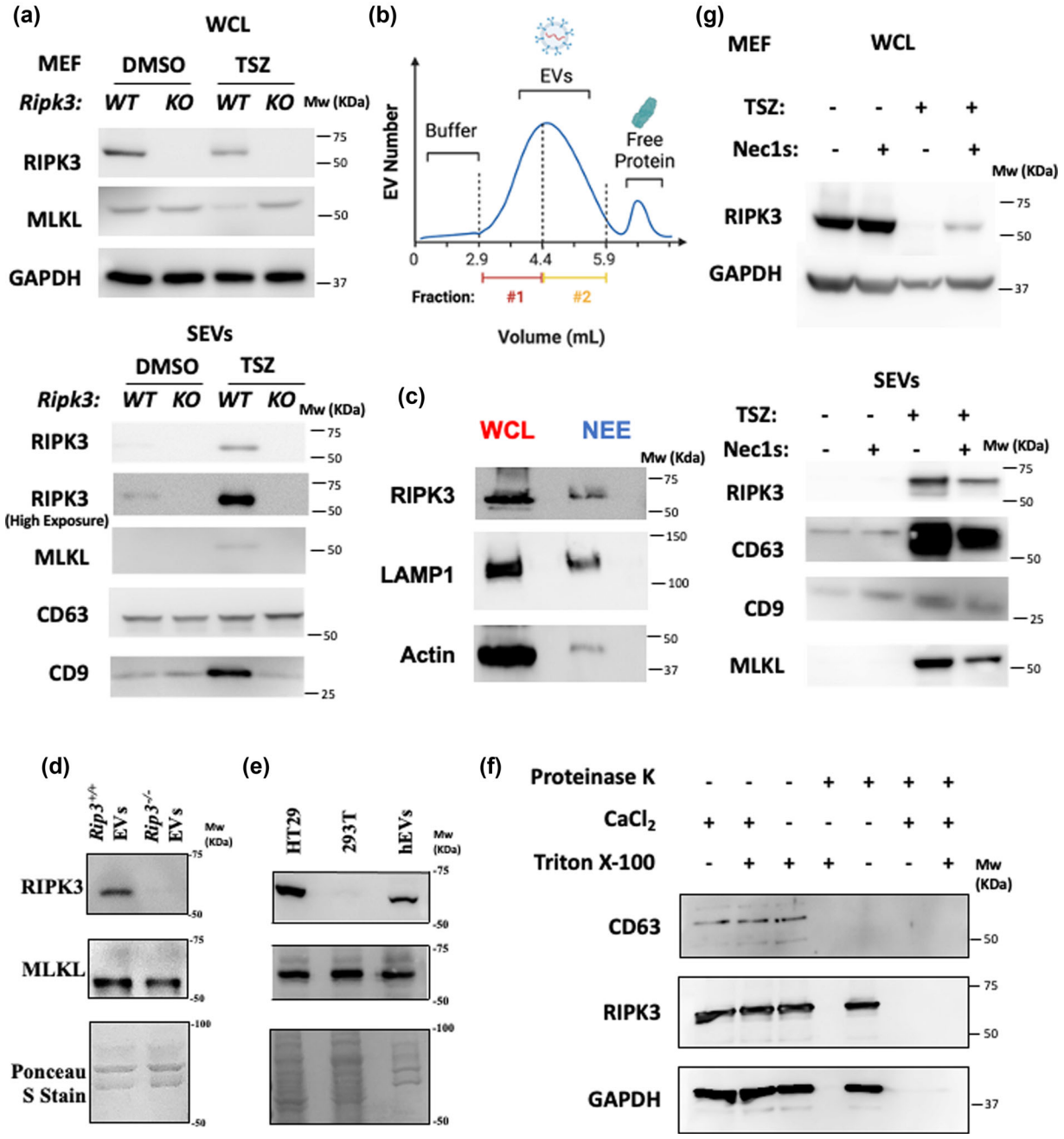

FIGURE 3 **RIPK3 is a luminal cargo protein in SEVs identifiable in diverse sources**. (a) *Ripk3*$^{+/+}$ and *Ripk3*$^{-/-}$ were treated with DMSO and TSZ. SEVs were isolated from cell culture. The whole-cell lysate (WCL) (top) and SEV fractions (bottom) were analyzed by western blotting. (b) Schematic outline showing size exclusion chromatography methodology for SEV enrichment. (c) Western blot analysis of SEVs purified using size exclusion chromatography. (d) SEVs were isolated from *Ripk3*$^{+/+}$ and *Ripk3*$^{-/-}$ mouse plasma and analyzed by western blotting for indicated proteins. Ponceau S staining was used to ensure equal protein amounts. (e) SEVs from human plasma were isolated and analyzed by western blotting. HT29 cells and 293T cells were used as positive and negative controls, respectively. Ponceau S staining was used to ensure equal protein amounts. (f) SEVs derived from TSZ treated *Ripk3*$^{+/+}$ MEFs were treated with proteinase K along with indicated reagents (see methods) and analyzed by western blotting. CD63 was used as a non-luminal (transmembrane) protein control whereas GAPDH was used as a luminal protein control. (g) *Ripk3*$^{+/+}$ and *Ripk3*$^{-/-}$ were treated with TSZ in the presence or absence of Nec1s. SEVs were isolated from cell culture and the cellular (left) and SEV fractions (right) were analyzed by western blotting

Next, we utilized HT29 cells—a commonly used human cell line in necroptosis assays—to confirm the presence of RIPK3 in SEVs. Similarly, RIPK3 was found to be enriched in SEVs from TSZ treated HT29 cells but not in cells treated with TS or T. Of note, TS or T alone was insufficient to induce necroptosis (Figure S2C). Further, we detected RIPK3 in SEVs isolated from mouse and human plasma (Figure S2E,F and Figure 3d,e). Notably, calnexin was not detected in HT-29 or MEF-derived SEVs further demonstrating low protein-contamination (Figure S2C,D).

To further rule out the possibility that RIPK3 is a non-specific protein contaminant that co-precipitates with SEVs, we tested whether RIPK3 resides within the lumen of SEVs using proteinase K protection assay, a commonly utilized technique (Brown et al., 2019). GAPDH (a previously reported luminal SEV protein) and CD63(a transmembrane protein) were included as controls. RIPK3 was "protected" against Proteinase K-dependent proteolytic cleavage but was degraded in the presence of triton-X100 which disrupts the vesicles (Figure 3f). Treating SEVs with $CaCl_2$ led to the loss of protection against proteinase K. These results indicate that RIPK3 resides within the lumen of SEVs and may be released when the vesicle membrane is disrupted.

We next inhibited upstream activation of RIPK3 via RIPK1 by utilizing Nec1s that prevents RIPK3 phosphorylation and subsequent necroptosis. Pre-treatment with Nec1s attenuated RIPK3 packaging inside SEV and "locked" RIPK3 inside the cells (Figure 3g). Curiously, administering NEEs to *Ripk3*$^{-/-}$ MEFs had no impact on cell-death under these experimental conditions (Figure S2G).

3.4 | NEE release during necroptosis is independent of Rab27a and Rab27b

The Rab27 family members RAB27a and b are required during SEV/ exosome release because of their roles in regulating vesicle fusion to the plasma membrane (Ostrowski et al., 2010). We procured Rab27a and b double knockout (Rab27DKO) mice originally generated by Miguel et al. and provided by O'Connell et al. (Alexander et al., 2017). MEFs isolated from Rab27WT or Rab27DKO mice showed a similar necroptosis response when treated with TSZ (Figure 4a). Next, we isolated SEVs from DMSO- and TSZ-treated WT or DKO MEFs and performed NTA analysis (Figure 4b) for SEV concentration and size. Under the DMSO condition, Rab27DKO reduced vesicle numbers without altering vesicle size distributions (Figure 4c,d). Both Rab27WT and Rab27DKO cells responded to TSZ with significantly elevated amounts of SEVs without significant alteration in SEV sizes (Figure 4c,d). Proteomics showed high levels of protein varieties in TSZ-treated cells, regardless of their Rab27 genotypes (Figure 4e, Table S2). However, subtle changes in protein cargos were noted. For example, vesicles from TSZ-treated Rab27WT cells had 137 unique proteins while the Rab27DKO group had 671 unique proteins (Figure 4e), suggesting that a selective Rab27-regulated process is involved in, in part in the release of cargo into SEVs. However, the release of RIPK3 into SEVs was determined by TSZ treatment rather than the Rab27 genotype (Figure 4f). Western blot analysis was in agreement with the NTA data. At the baseline (DMSO-treated cells), Rab27 double knockout reduced the levels of RIPK3 detected in SEVs (Figure 4g). Similar to what we described earlier, TSZ treatment dramatically elevated RIPK3 in SEVs from Rab27WT cells. Surprisingly, Rab27 double knockout had no effects on RIPK3s detected in SEVs from necroptotic cells (Figure 4g). These data suggest that the majority of protein cargos including RIPK3 are shuttled into SEVs during necroptosis via a mechanism that is independent of Rab27a/b, which is contrasting to healthy cells.

3.5 | Rab11b interacts with RIPK3 within NEEs

Given the role of the Rab family of proteins in vesicular trafficking, we sought to identify other Rab proteins that may regulate the release of SEVs during necroptosis in a RIPK3-dependent manner. Close examinations of our proteomic data revealed the presence of several Rab-family members in SEVs including Rab21, Rab6a, Rab6b, Rab18 and others Rab11a and Rab11b. Rab11 isoforms—Rab11a, Rab11b, and Rab25—have previously been found in SEVs including those secreted by necroptotic cells (Shlomovitz et al., 2021). To address whether RIPK3 and Rab11 could be mechanistically involved in SEV release during necroptosis, we immunoprecipitated extract from WCL and NEEs with an anti-RIPK3 antibody and subjected the resulting complexes to mass-spectrometry analysis. Among the proteins that co-immunoprecipitated with RIPK3, Rab11b was highly enriched in SEVs derived from TSZ-treated cells (Figure 5a, Table S3). Among the NEE-associated proteins pulled down by anti-RIPK3, several have previously reported relation to RIPK3. STRING analysis of these proteins showed strong calcium-dependency such as CamKII, Capn2 and others (Figure 5b). Previously, a calcium-dependent form of atypical SEV exocytosis has been found to occur via the lysosomes—lysosomal exocytosis. Therefore, we analyzed lysosome-associated proteins from SEVs derived from DMSO and TSZ treated MEFs. We found that necroptosis is associated with a vast increase in lysosomal proteins, some of which are shared with the DMSO group (Figure 5c, Tables 1 and S4). Surprisingly, no unique lysosomal proteins were found in the DMSO alone group. The increase in lysosomal proteins in NEEs suggests that necroptosis may switch the SEV release from a Rab27-dependent mechanism to a lysosomal exocytosis mechanism.

3.6 | NEE release is dependent upon calcium

We hypothesize that the calcium-dependent process of lysosomal exocytosis underlies SEV release during necroptosis. We used the calcium chelator BAPTA-AM or calcium-free culture media to perturb the calcium-dependent processes. Depletion of calcium led to a moderate but significant attenuation of necroptosis as measured by flow cytometry at 6 h post treatment (Figure 6a

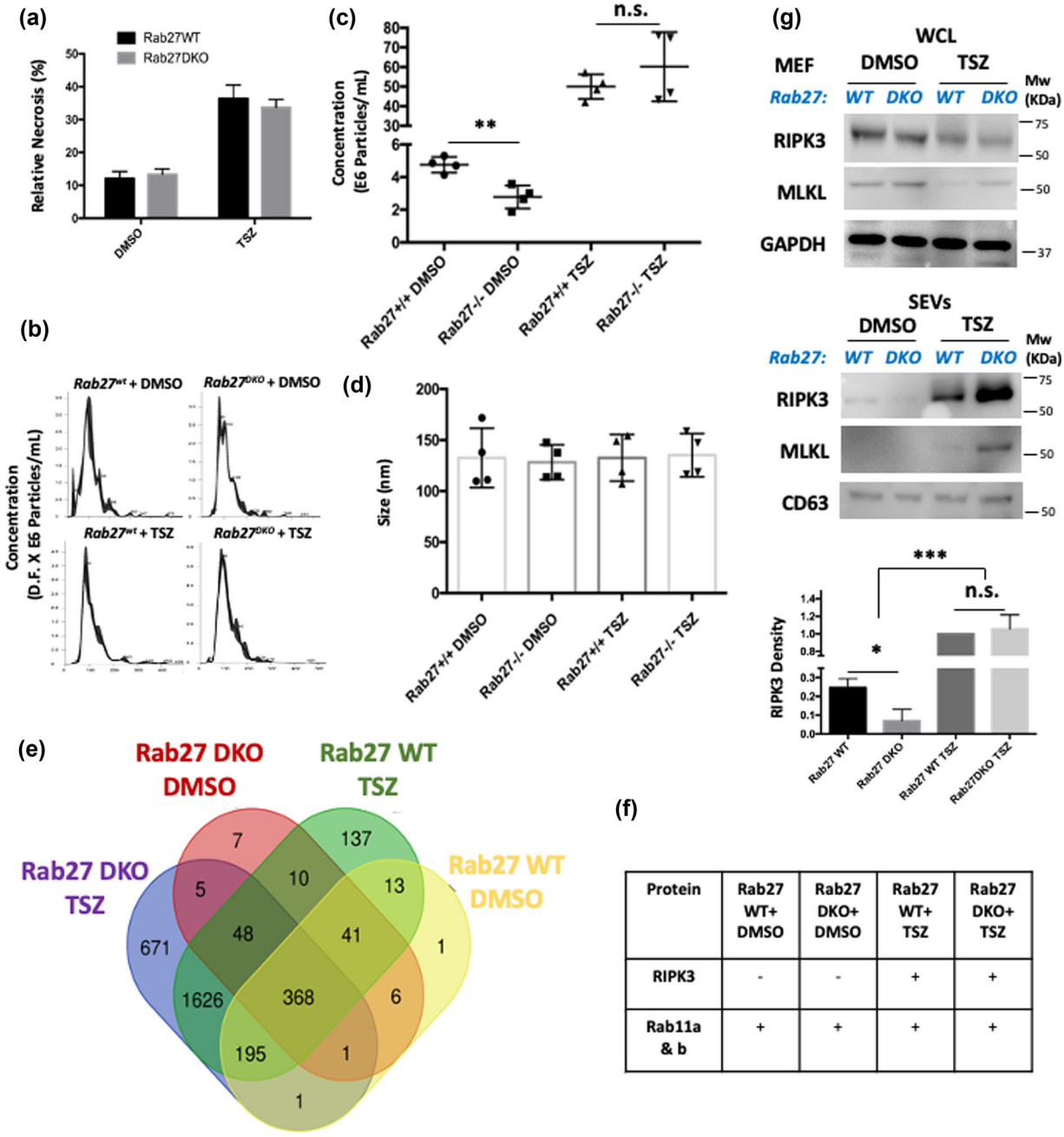

(f)

Protein	Rab27 WT+ DMSO	Rab27 DKO+ DMSO	Rab27 WT+ TSZ	Rab27 DKO+ TSZ
RIPK3	-	-	+	+
Rab11a & b	+	+	+	+

FIGURE 4 **NEE release is independent of Rab27a/b.** (a) MEFs from *Rab27WT* and *Rab27DKO* were treated with DMSO and TSZ and cell death is analyzed by flow cytometry. Relative necrosis is depicted. (b–d) SEVs from DMSO or TSZ treated *Rab27WT* and *Rab27DKO* MEFs were isolated by ultracentrifugation and analyzed by NTA. Representative NTA trace is presented (b). The number of particles (c) and the mean size is plotted (d). (e) SEVs isolated in (a) were subjected to mass spectrometry analysis and the number of protein cargo is depicted in a Venn diagram. (f) Comparison of RIPK3 and Rab11a/b enrichment in SEVs from the mass spectrometry in € analysis is presented. "+" represents the detection of the indicated factor by mass spectrometry whereas "-" indicates its absence. (g) WCL and SEVs from *Rab27WT* and *Rab27DKO* MEFs treated with DMSO and TSZ were analyzed by western blotting. RIPK3 abundance was analyzed in SEVs by densitometry and quantified. All data shown are mean ± SD of three or more independent experiments. $^{*}p < 0.05$, $^{**}p < 0.01$ $^{***}p < 0.001$ using one-way ANOVA (c, g)

and S3). However, calcium depletion did not alter upstream necroptosis signalling as phosphorylated MLKL levels (at 1 h) remained constant in necroptotic cells with or without calcium depletion (Figure 6b). When analyzed by NTA, calcium depletion had no overall impact on SEV size but led to a significant decrease in the number of secreted SEVs released by necroptotic cells (Figure 6c,d). Western blotting showed that calcium depletion led to a decrease in SEV-associated RIPK3 as well as MLKL (Figure 6e,f).

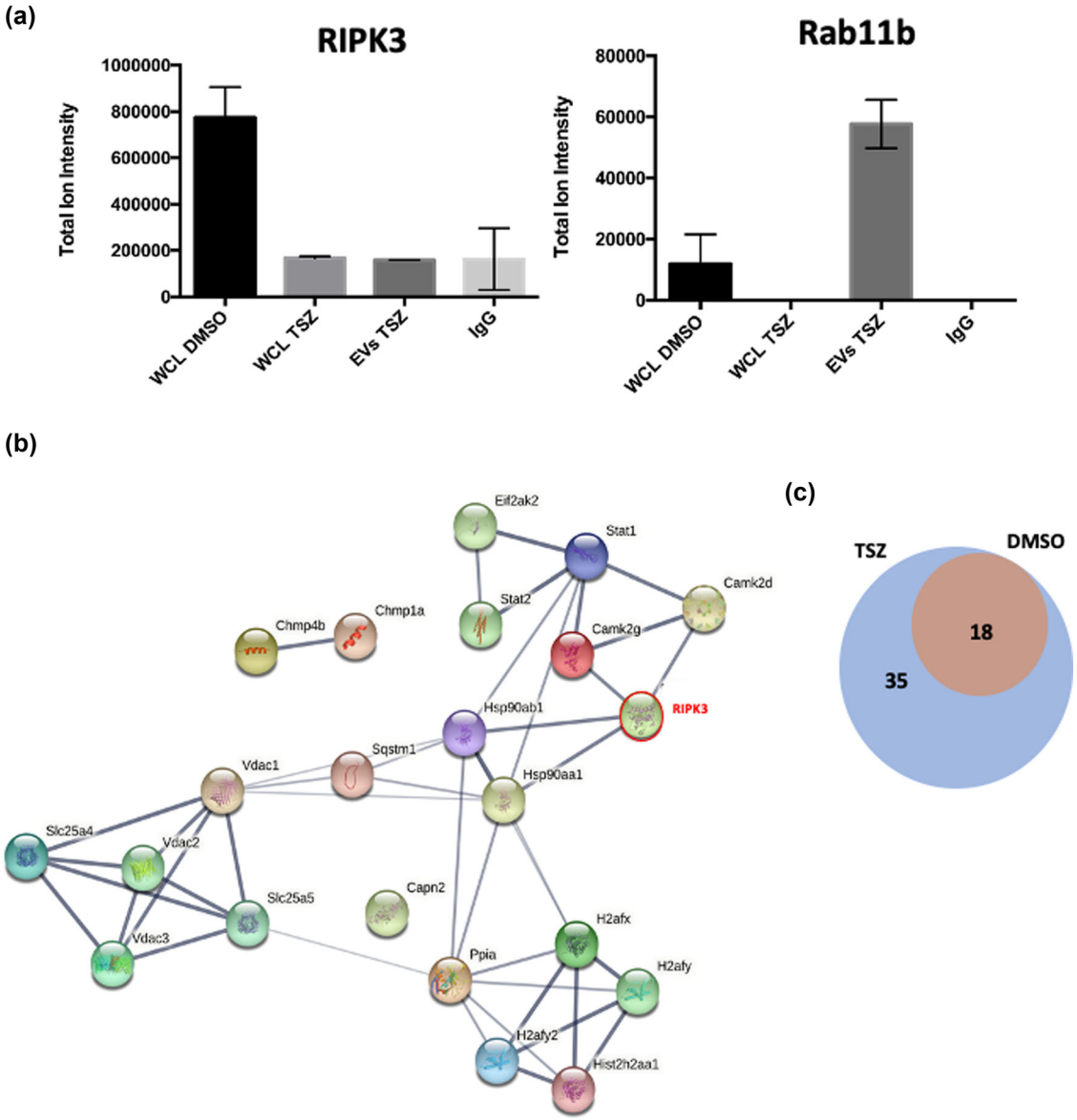

FIGURE 5 **RIPK3 is released in an atypical manner during necroptosis**. (a) Immunoprecipitation experiment was performed using RIPK3 or IgG on DMSO treated (DMSO WCL) and TSZ treated (WCL TSZ) MEFs, or SEVs derived from TSZ treated MEFs (EVs TSZ) and analyzed by mass spectrometry. The fold enrichment of RIPK3 and Rab11b from the co-immunoprecipitated is depicted from 3 independent replicates ($n = 3$). (b) STRING analysis was performed for RIPK3 interacting proteins identified in RIPK3 IP coupled mass spectrometry leading to the identification of known or predicted interaction partners. Note that many interacting partners are calcium-binding proteins. (c) Analysis of known lysosomal proteins enriched in SEVs derived from TSZ or DMSO treated MEFs are represented as a Venn diagram

3.7 | Abrogating lysosomal exocytosis by Vacuolin-1 attenuates RIPK3 being released into SEVs

To directly test the role of lysosomal exocytosis in sorting RIPK3 to SEVs during necroptosis, we utilized a highly specific inhibitor of lysosomal exocytosis Vacuolin-1 (Huynh & Andrews, 2005). Similar to calcium depletion, Vacuolin-1 pretreatment led to attenuated necrosis measured by flow cytometry at 6 h without affecting the phosphorylation of MLKL at 1 h post treatment (Figure 7a,b). When SEVs derived from such treated cells were subject to NTA analysis, Vacuolin-1 caused a wide size variation (Figure 7c). Western blotting showed that Vacuolin-1 treatment led to a decrease in RIPK3 levels in the NEEs (Figure 7d,e).

4 | DISCUSSION

During necroptosis, an increase in the production of SEVs is known to occur (Yoon et al., 2017). SEV biogenesis during necroptosis is a well-orchestrated process. Due to its link to necroptosis, the discovery of MLKL in SEV biogenesis partly describes the

TABLE 1 List of lysosomal proteins found enriched in SEVs isolated from MEFs treated with DMSO (column 1), TSZ treated (column 2) or those found common in both (column 3)

Lysosome (Untreated)	Lysosome (Treated)	Lysosome (Both)
	Ank3	Aldob
	Asah1	Apoe
	Cd63	Bin1
	Cdip1	Cd81
	Chmp5	Hexa
	Clcn7	Hexb
	Ehd3	Myh9
	Epdr1	Prdx6
	Fnbp1	Rab14
	Fyco1	Rab21
	Gak	Rock2
	Gcc2	Rtn4
	Hdac6	Snx2
	Hgs	Src
	Hook3	Stx8
	Irgm1	Szt2
	Ldlr	Vps35
	Mfsd1	Wdr81
	Mtor	
	Nbr1	
	Rab34	
	Rhob	
	Sec13	
	Sidt2	
	Snx6	
	Stx7	
	Tsc2	
	Vamp2	
	Vamp8	
	Vps11	
	Vps18	
	Vps25	
	Vps41	
	Vps51	
	Wdr91	

Note: No unique proteins were found in DMSO (i.e., untreated) conditions.

mechanism of production of these necroptotic SEVs; however, MLKL can also regulate SEV biogenesis in cells naturally lacking RIPK3 (Yoon et al., 2017) and independent of necroptosis induction. Our data suggest that RIPK3 might be more fundamentally involved in the mechanism of generation of these necroptotic SEVs and may redirect the mode of SEV release through MLKL-mediated calcium influx and activation of lysosomal exocytosis (Figure 8).

The presence of RIPK3 within SEVs was supported by our proteomic analysis and Western blotting experiments. Compared to healthy cells, cells undergoing necroptosis released SEVs that contained more diverse cargo proteins. Furthermore, the packaging of proteins into necroptosis-associated SEVs appeared to be an active process, with preferences for proteins involved in certain pathways such as membrane trafficking and RNA metabolism, rather than randomly packaging any intracellular proteins as it might be in the situation of cellular debris. The physical properties of SEVs from necroptosis were similar to those released by

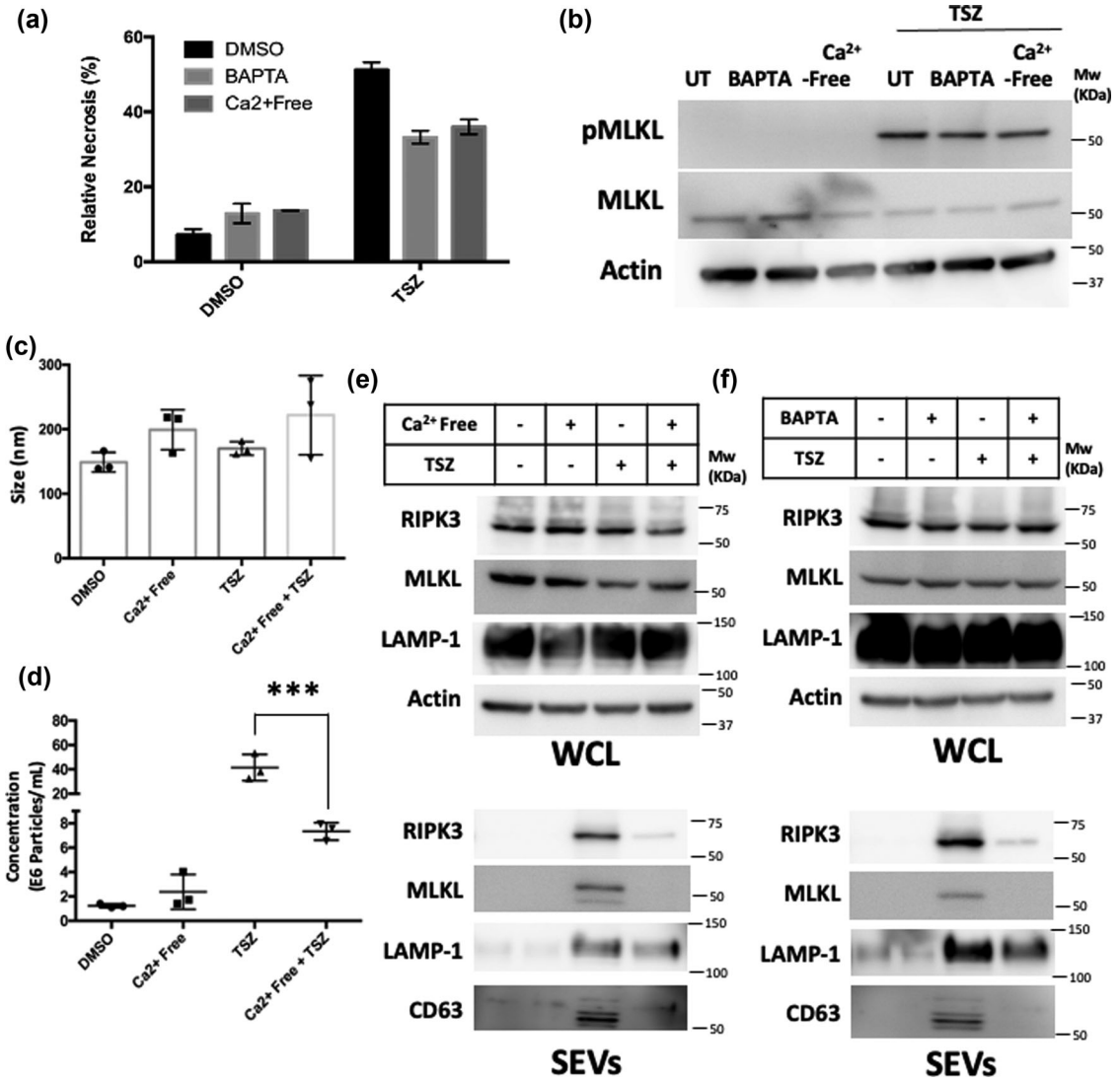

FIGURE 6 **NEEs are released in a calcium-dependent manner.** (a) MEFs were cultured in calcium-containing or calcium-free media or pre-treated with the calcium chelator BAPTA. Necroptosis was induced using TSZ. The percentage of necroptotic cells is plotted. (b) Early activation of necroptosis is measured by using pMLKL. Briefly, MEFs cultured in indicated conditions were treated with DMSO or TSZ for 1 h and harvested for western blot analysis. (c, d) NTA analysis was performed on SEVs isolated from MEFs cultured in calcium-containing or calcium-free media and subsequent treatment with DMSO or TSZ for mean size (c) and concentration (d). (e) Using a cell culture strategy similar to (a), WCL (up) and SEVs (below) were analyzed for RIPK3 abundance by western blotting. LAMP-1 was used as a marker for lysosomal exocytosis. (Machado et al., 2015; Mathieu et al., 2021; Park et al., 2018) All data shown are mean ± SD of three or more independent experiments. ***$p < 0.001$ using one-way ANOVA (d)

healthy cells. Both EM and NTA showed that SEVs—isolated by two different methods—have similar size distributions regardless of their RIPK3 genotypes or whether they were undergoing necroptosis. NEEs appear to share about half the proteins (1023) identified in similar NEEs in macrophages (Shlomovitz et al., 2021) although RIPK3 was uniquely identified in our study (Table S5).

Rab27a and Rab27b have been known for their essential role in the biogenesis of SEVs such as exosomes (Ostrowski et al., 2010). Consistent with the literature, Rab27DKO MEFs released fewer SEVs under baseline compared to their wild-type counterparts. However, the release of SEVs by necroptotic cells showed insensitivity to the loss of Rab27a/b. In fact, during necroptosis, the loss of Rab27 did not affect the enhanced SEV release nor the heightened RIPK3 packaging inside SEVs, suggesting that packaging and release of SEVs may occur via different routes depending on cellular health.

Lysosomal exocytosis is a calcium-dependent process in which a ruptured plasma membrane is immediately sealed by the fusion of the lysosomes to prevent the spread of necrosis to the entire cell (Jaiswal et al., 2002; Reddy et al., 2001). Recently, lysosomal exocytosis was implicated in necroptosis; however, it remained unclear whether this had any effect on cell death and the generation of SEVs itself. In our study, blocking lysosomal exocytosis by depleting calcium or by using Vacuolin-1 blunted the necroptosis-enhanced SEV release and the RIPK3 incorporation into SEVs. This finding suggests that necroptosis induction

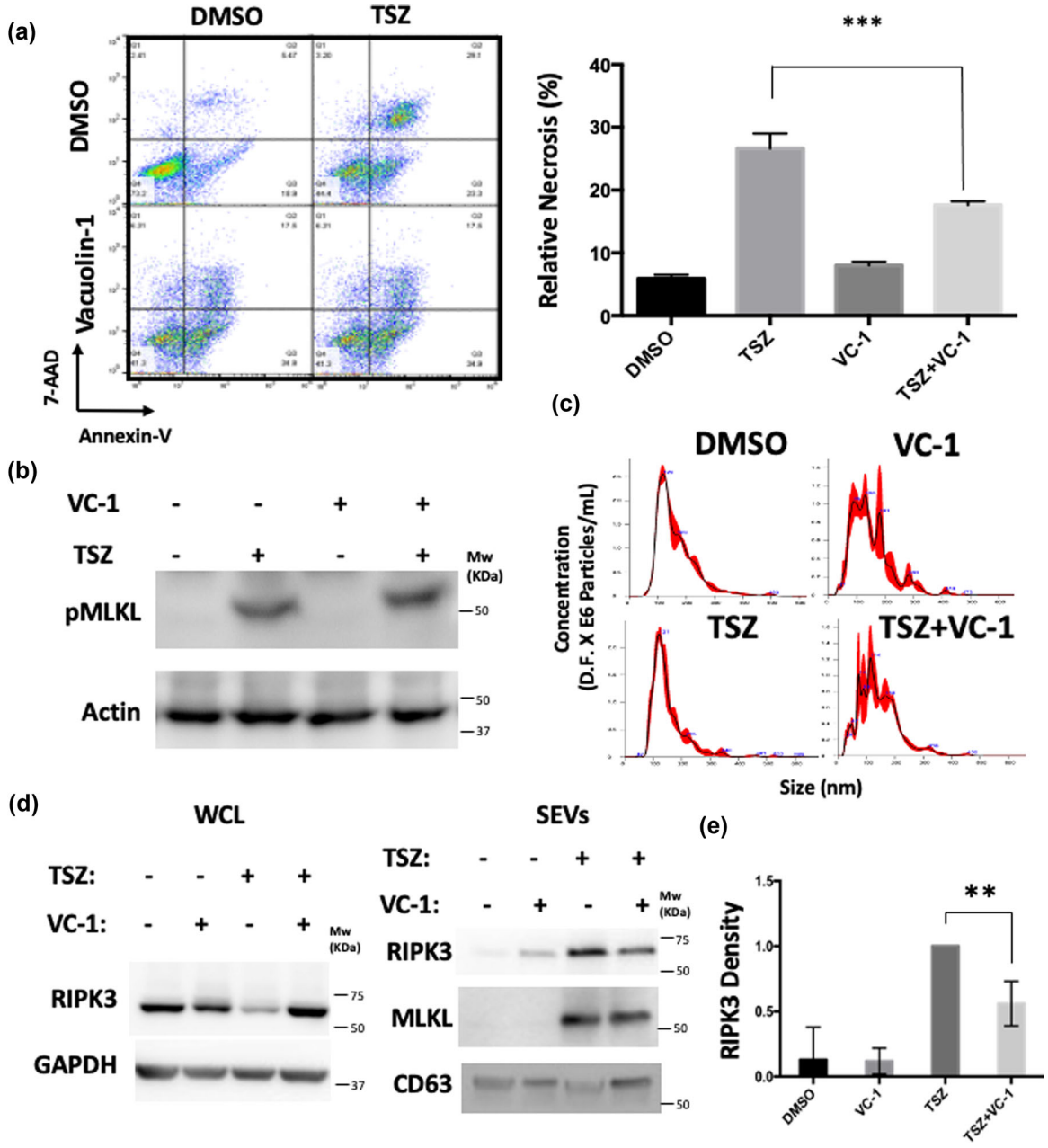

FIGURE 7 **Necroptosis leads to the lysosomal-mediated secretion of RIPK3 carrying SEVs.** (a) MEFs were pretreated with DMSO or Vacuolin-1 and subsequently with DMSO or TSZ and analyzed by flow cytometry. The resulting scatter plot is depicted (left) and percent necrosis is plotted (right). (b) Early activation of necroptosis was assessed by the abundance of phosphorylated MLKL (pMLKL). Briefly, MEFs pre-treated with VC-1 or DMSO and subsequently induced with DMSO or TSZ for 1 h were harvested for western blot analysis. (c) MEFs were pre-treated with VC-1 or DMSO and subsequently induced with DMSO or TSZ. SEVs were isolated using ultracentrifugation and analyzed by NTA and a representative trace is depicted. (d) MEFs were treated similarly to (c). WCL (left) and SEVs (right) were analyzed by western blotting. (e) RIPK3 levels in SEVs were quantified by densitometry and plotted. All data shown are mean ± SD of three or more independent experiments. *$p < 0.01$, ***$p < 0.001$ using one-way ANOVA (a, e)

greatly activates lysosome-mediated extrusion and may in fact be responsible for the increase in SEV numbers. The effects of endosome-mediated SEV expulsion may be masked by lysosomal exocytosis; therefore, it remains to be determined whether the endosomal route of SEV extrusion is completely dismantled during necroptosis.

The dual role of MLKL in RIPK3-independent SEV biogenesis, as well as in membrane rupture currently makes it technically challenging to ascertain whether RIPK3 and MLKL can be released in NEEs independent of membrane rupture and MLKL mediated Calcium influx. Silencing MLKL expression or its pharmacological inhibition to prevent plasma membrane rupture are expected to abrogate vesicular trafficking. Future efforts utilizing the genetic and biochemical understanding of MLKL protein that uncouple its role in SEV-biogenesis and membrane rupture will be valuable in this understanding. Further, a recent study

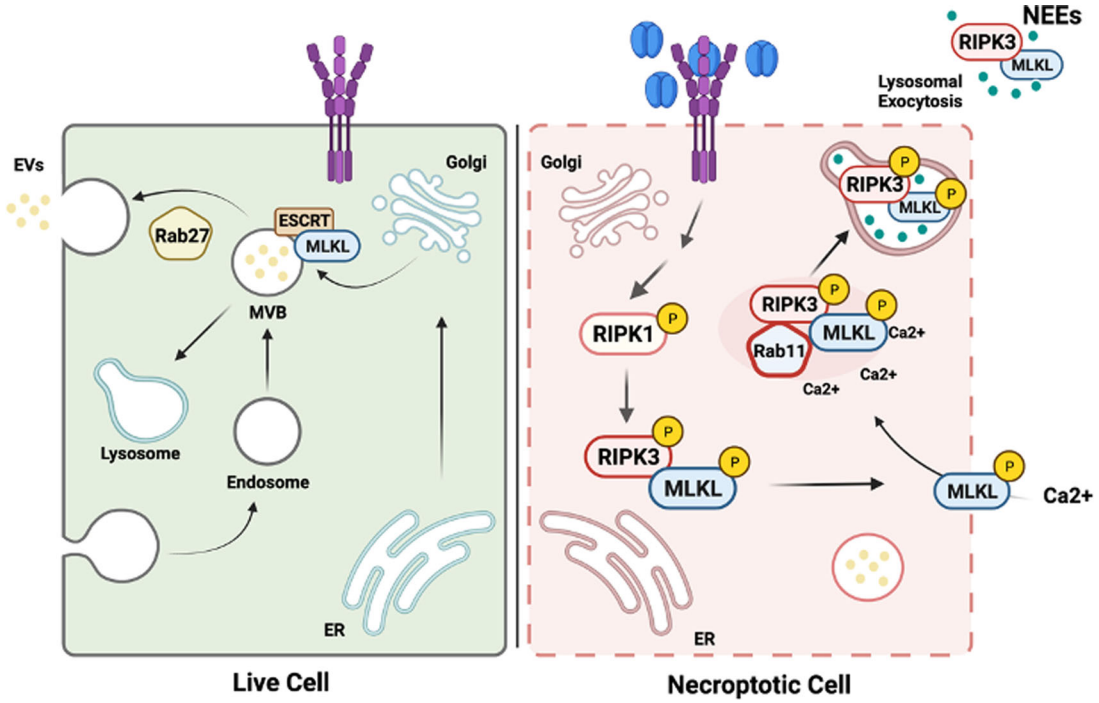

FIGURE 8 **Proposed model for NEE generation**. *Left*: in a healthy cell, SEV generation occurs through the endosomal machinery that involves early and late endosome formation and fusion with the MVBs involving ESCRT proteins and MLKL. Many of the endosomal maturation steps are regulated by the Rab-family of proteins but the terminal steps of fusion to the plasma membrane, mediated by Rab27 (Rab27a and Rab27b) is denoted. *Right*: Upon engagement of TNF-α with TNFR, activation of RIPK1, RIPK3 and MLKL via phosphorylation activates a Rab27-independent program of lysosomal exocytosis where Rab11 interacts with RIPK3 and triggers the secretion of NEEs as a result of calcium influx secondary to MLKL-mediated plasma membrane damage

identified a role of Rab27 in linking MLKL activation to terminal necrosis via Pannexin-1 (Douanne et al., 2019). In their study, Douanne et al. found that knocking down Rab27a or Rab27b led to a decrease in the plasma membrane "leakiness" dependent on MLKL which also impacted SEV number. In our study, we identify in Rab27DKO MEFs that although baseline SEV biogenesis was abrogated, this difference was lost upon necroptosis induction. The use of HT29 (a cancer cell line) or differences in techniques to measure SEV numbers may explain the differences in our observations. Regardless, in agreement with this report, we do not observe any notable differences in cell death propensities in Rab27WT and Rab27DKO MEFs.

The endosomal trafficking machinery dynamically exchanges cargo with the lysosomes and is determined by other Rab family GTPases. Key proteins like RIPK3 and MLKL have already been shown to be associated with the lysosomes. For instance, RIPK3 when ubiquitinated by CHIP is degraded in the lysosomes (Seo et al., 2016). Recently, it was also shown that MLKL can be trafficked back for degradation in the lysosomes via lipid rafts; surprisingly, this report also demonstrated that MLKL can alternatively be expelled from cells via SEVs (Fan et al., 2019). Although studying how RIPK3 is incorporated inside lysosomal SEVs is beyond the scope of our current study, the mechanisms above demonstrate that these proteins are indeed found in lysosomes. Towards this, we analyzed our MS data in SEVs along with data deposited by others. We and others (Shlomovitz et al., 2021) find Rab11 to be repeatedly enriched in SEVs from necrotic cells and was independently found to co-immunoprecipitate with RIPK3 (Zhang et al., 2009). Rab11 has previously been shown to control the homeostasis of endosomal and lysosomal maturation (Zulkefli et al., 2019) and together with its interaction with phospho RIPK3 (Zhang et al., 2009) is an attractive candidate for "switching" the mode of SEV production from endosome to lysosome. Indeed, Rab11 and its associated family members are known to be phosphorylated and may be dependent on RIPK3.

Our study utilizes MEFs and HT-29 which are a commonly used (murine) primary and (human) cancer cell types, respectively, for necroptosis studies (Liccardi et al., 2019; Najafov et al., 2019; Yoon et al., 2017). Several other cell types have epigenetically silenced RIPK3, and therefore unsuitable for necroptosis studies (Koo et al., 2015; Wang et al., 2020) due to their inability to undergo this form of cell death. Further, we utilized MEFs due to the ease of isolation from a wide variety of knock-out mouse models, such as Rab27a/b and RIPK3 in the current study, and their wide usage in mechanistic studies related to SEVs (Liccardi et al., 2019; Najafov et al., 2019; Yoon et al., 2017). Although the cell-specific differences may occur, due to the well preserved necroptotic machinery (RIPK3 and MLKL) in many primary tissues, the production of NEEs through this atypical mechanism may be expected. In support of this, previous studies have found similar enhancement of SEV-production and MLKL release in other cell types (Yoon et al., 2017). Lastly, RIPK3 and MLKL have been found in plasma isolated from various mouse models and

human diseases even though their presence in SEVs was not tested. These data suggest that the release of RIPK3 and MLKL in NEEs are likely to be a ubiquitous phenomenon.

Taken together, we identify for the first time that necroptosis is associated with the release of SEVs that contain RIPK3 and MLKL in addition to many other unique proteins. Further, we demonstrate that during necroptosis, SEV release via lysosomal exocytosis is preferred over the more conventional MVB-mediated exocytosis. This alternate mode of exocytosis is responsible for an acute increase in SEV release during necroptosis as observed by us and others. The biological function of the release of RIPK3 and MLKL in SEVs is unclear but may be a part of the cellular defence against necroptosis.

ACKNOWLEDGEMENTS

We acknowledge the generosity of Dr. Miguel C Seabra, Imperial College London and Dr. Ryan O'Connell, University of Utah for respectively generating Rab27DKO mice and sharing the breeder mice. We also acknowledge the help of Alissa Weaver, MD, PhD, of Vanderbilt University in EV isolation and characterization. This study was supported by the National Institutes of Health R01HL149404 (B.L), NIH R01GM125085 (Y.G), R01GM117058 (Y.G), and S10OD018475 (Y.G), American Heart Association 20TPA35490307 (B.L), 17PRE33670082 (KG), Vascular Surgery Research Training Program Grant T32 HL110853 (K.A.B and M.K.K), American Heart Association Predoctoral Fellowship (D.S.R). The funders had no role in study design, data collection and analysis, decision to publish, or preparation of the manuscript. Schematic figures were created with BioRender.com.

CONFLICT OF INTEREST STATEMENT

KAB and YG are co-inventors on a patent that covers the detergent Azo. Other authors have no conflict of interest to declare.

REFERENCES

Aballo, T. J., Roberts, D. S., Melby, J. A., Buck, K. M., Brown, K. A., & Ge, Y. (2021). Ultrafast and reproducible proteomics from small amounts of heart tissue enabled by Azo and timsTOF pro. *Journal of Proteome Research*, *20*, 4203–4211. https://doi.org/10.1021/acs.jproteome.1c00446

Alexander, M., Ramstead, A. G., Bauer, K. M., Lee, S. - H., Runtsch, M. C., Wallace, J., Huffaker, T. B., Larsen, D. K., Tolmachova, T., Seabra, M. C., Round, J. L., Ward, D. M., & O'Connell, R. M. (2017). Rab27-dependent exosome production inhibits chronic inflammation and enables acute responses to inflammatory stimuli. *Journal of Immunology*, *199*, 3559–3570. https://doi.org/10.4049/jimmunol.1700904

Brown, K. A., Chen, B., Guardado-Alvarez, T. M., Lin, Z., Hwang, L., Ayaz-Guner, S., Jin, S., & Ge, Y. (2019). A photocleavable surfactant for top-down proteomics. *Nature Methods*, *16*(5), 417–420. https://doi.org/10.1038/s41592-019-0391-1

Brown, K. A., Tucholski, T., Eken, C., Knott, S., Zhu, Y., Jin, S., & Ge, Y. (2020a). High-throughput proteomics enabled by a photocleavable surfactant. *Angewandte Chemie*, *132*, 8484–8488. https://doi.org/10.1002/ange.201915374

Brown, K. A., Tucholski, T., Eken, C., Knott, S., Zhu, Y., Jin, S., & Ge, Y. (2020b). High-throughput proteomics enabled by a photocleavable surfactant. *Angewandte Chemie International Edition*, *59*, 8406–8410. https://doi.org/10.1002/anie.201915374

Cai, Z., Jitkaew, S., Zhao, J., Chiang, H. - C., Choksi, S., Liu, J., Ward, Y., Wu, L. - G., & Liu, Z. - G. (2014). Plasma membrane translocation of trimerized MLKL protein is required for TNF-induced necroptosis. *Nature Cell Biology*, *16*, 55–65. https://doi.org/10.1038/ncb2883

Cho, Y., Challa, S., Moquin, D., Genga, R., Ray, T. D., Guildford, M., & Chan, F. K. - M. (2009). Phosphorylation-driven assembly of the RIP1-RIP3 complex regulates programmed necrosis and virus-induced inflammation. *Cell*, *137*, 1112–1123. https://doi.org/10.1016/j.cell.2009.05.037

Douanne, T., André-Grégoire, G., Trillet, K., Thys, A., Papin, A., Feyeux, M., Hulin, P., Chiron, D., Gavard, J., & Bidère, N. (2019). Pannexin-1 limits the production of proinflammatory cytokines during necroptosis. *EMBO Reports*, *20*, e47840. https://doi.org/10.15252/embr.201947840

Fan, W., Guo, J., Gao, B., Zhang, W., Ling, L., Xu, T., Pan, C., Li, L., Chen, S., Wang, H., Zhang, J., & Wang, X. (2019). Flotillin-mediated endocytosis and ALIX-syntenin-1-mediated exocytosis protect the cell membrane from damage caused by necroptosis. *Science Signaling*, *12*, eaaw3423. https://doi.org/10.1126/scisignal.aaw3423

Fukuda, M. (2013). Rab27 effectors, pleiotropic regulators in secretory pathways. *Traffic (Copenhagen, Denmark)*, *14*, 949–963. https://doi.org/10.1111/tra.12083

Gong, Y. - N., Guy, C., Olauson, H., Becker, J. U., Yang, M., Fitzgerald, P., Linkermann, A., & Green, D. R. (2017). ESCRT-III acts downstream of MLKL to regulate necroptotic cell death and its consequences. *Cell*, *169*, 286–300.e16. https://doi.org/10.1016/j.cell.2017.03.020

Grosshans, B. L., Ortiz, D., & Novick, P. (2006). Rabs and their effectors: Achieving specificity in membrane traffic. *Proceedings of the National Academy of Sciences of the United States of America*, *103*, 11821–11827. https://doi.org/10.1073/pnas.0601617103

Harmati, M., Gyukity-Sebestyen, E., Dobra, G., Janovak, L., Dekany, I., Saydam, O., Hunyadi-Gulyas, E., Nagy, I., Farkas, A., Pankotai, T., Ujfaludi, Z., Horvath, P., Piccinini, F., Kovacs, M., Biro, T., & Buzas, K. (2019). Small extracellular vesicles convey the stress-induced adaptive responses of melanoma cells. *Science Reports*, *9*, 15329. https://doi.org/10.1038/s41598-019-51778-6

He, S., Wang, L., Miao, L., Wang, T., Du, F., Zhao, L., & Wang, X. (2009). Receptor interacting protein kinase-3 determines cellular necrotic response to TNF-alpha. *Cell*, *137*, 1100–1111. https://doi.org/10.1016/j.cell.2009.05.021

Hildebrand, J. M., Tanzer, M. C., Lucet, I. S., Young, S. N., Spall, S. K., Sharma, P., Pierotti, C., Garnier, J. - M., Dobson, R. C. J., Webb, A. I., Tripaydonis, A., Babon, J. J., Mulcair, M. D., Scanlon, M. J., Alexander, W. S., Wilks, A. F., Czabotar, P. E., Lessene, G., Murphy, J. M., & Silke, J. (2014). Activation of the pseudokinase MLKL unleashes the four-helix bundle domain to induce membrane localization and necroptotic cell death. *Proceedings of the National Academy of Sciences*, *111*, 15072. https://doi.org/10.1073/pnas.1408987111

Huynh, C., & Andrews, N. W. (2005). The small chemical vacuolin-1 alters the morphology of lysosomes without inhibiting Ca2+-regulated exocytosis. *EMBO Reports*, *6*, 843–847. https://doi.org/10.1038/sj.embor.7400495

Jaiswal, J. K., Andrews, N. W., & Simon, S. M. (2002). Membrane proximal lysosomes are the major vesicles responsible for calcium-dependent exocytosis in nonsecretory cells. *Journal of Cell Biology*, *159*, 625–635. https://doi.org/10.1083/jcb.200208154

Keerthikumar, S., Chisanga, D., Ariyaratne, D., Al Saffar, H., Anand, S., Zhao, K., Samuel, M., Pathan, M., Jois, M., Chilamkurti, N., Gangoda, L., & Mathivanan, S. (2016). ExoCarta: A web-based compendium of exosomal cargo. *Journal of Molecular Biology*, *428*, 688–692. https://doi.org/10.1016/j.jmb.2015.09.019

Koo, G. - B., Morgan, M. J., Lee, D. - G., Kim, W. - J., Yoon, J. - H., Koo, J. S., Kim, S. I., Kim, S. J., Son, M. K., Hong, S. S., Levy, J. M. M., Pollyea, D. A., Jordan, C. T., Yan, P., Frankhouser, D., Nicolet, D., Maharry, K., Marcucci, G., Choi, K. S., … Kim, Y.-S. (2015). Methylation-dependent loss of RIP3 expression in cancer represses programmed necrosis in response to chemotherapeutics. *Cell Research*, *25*, 707–725. https://doi.org/10.1038/cr.2015.56

Liccardi, G., Ramos Garcia, L., Tenev, T., Annibaldi, A., Legrand, A. J., Robertson, D., Feltham, R., Anderton, H., Darding, M., Peltzer, N., Dannappel, M., Schünke, H., Fava, L. L., Haschka, M. D., Glatter, T., Nesvizhskii, A., Schmidt, A., Harris, P. A., Bertin, J., … Meier, P. (2019). RIPK1 and caspase-8 ensure chromosome stability independently of their role in cell death and inflammation. *Molecular Cell*, *73*, 413–428.e7. https://doi.org/10.1016/j.molcel.2018.11.010

Machado, E., White-Gilbertson, S., Van De Vlekkert, D., Janke, L., Moshiach, S., Campos, Y., Finkelstein, D., Gomero, E., Mosca, R., Qiu, X., Morton, C. L., Annunziata, I., & d'Azzo, A. (2015). Regulated lysosomal exocytosis mediates cancer progression. *Science Advances*, *1*, e1500603. https://doi.org/10.1126/sciadv.1500603

Mathieu, M., Névo, N., Jouve, M., Valenzuela, J. I., Maurin, M., Verweij, F. J., Palmulli, R., Lankar, D., Dingli, F., Loew, D., Rubinstein, E., Boncompain, G., Perez, F., & Théry, C. (2021). Specificities of exosome versus small ectosome secretion revealed by live intracellular tracking of CD63 and CD9. *Nature Communication*, *12*, 4389. https://doi.org/10.1038/s41467-021-24384-2

Meier, F., Brunner, A.-D., Koch, S., Koch, H., Lubeck, M., Krause, M., Goedecke, N., Decker, J., Kosinski, T., Park, M. A., Bache, N., Hoerning, O., Cox, J., Räther, O., & Mann, M. (2018). Online parallel accumulation-serial fragmentation (PASEF) with a novel trapped ion mobility mass spectrometer. *Molecular & Cellular Proteomics*, *17*, 2534–2545. https://doi.org/10.1074/mcp.TIR118.000900

Najafov, A., Mookhtiar, A. K., Luu, H. S., Ordureau, A., Pan, H., Amin, P. P., Li, Y., Lu, Q., & Yuan, J. (2019). TAM kinases promote necroptosis by regulating oligomerization of MLKL. *Molecular Cell*, *75*, 457–468.e454. https://doi.org/10.1016/j.molcel.2019.05.022

Ostrowski, M., Carmo, N. B., Krumeich, S., Fanget, I., Raposo, G., Savina, A., Moita, C. F., Schauer, K., Hume, A. N., Freitas, R. P., Goud, B., Benaroch, P., Hacohen, N., Fukuda, M., Desnos, C., Seabra, M. C., Darchen, F., Amigorena, S., Moita, L. F., & Thery, C. (2010). Rab27a and Rab27b control different steps of the exosome secretion pathway. *Nature Cell Biology*, *12*, 19–30. sup pp 11–13. https://doi.org/10.1038/ncb2000

Park, S. J., Kim, J. M., Kim, J., Hur, J., Park, S., Kim, K., Shin, H.-J., & Chwae, Y.-J. (2018). Molecular mechanisms of biogenesis of apoptotic exosome-like vesicles and their roles as damage-associated molecular patterns. *Proceedings of the National Academy of Sciences of the United States of America*, *115*, E11721–e11730. https://doi.org/10.1073/pnas.1811432115

Pathan, M., Fonseka, P., Chitti, S. V., Kang, T., Sanwlani, R., Van Deun, J., Hendrix, A., & Mathivanan, S. (2019). Vesiclepedia 2019: A compendium of RNA, proteins, lipids and metabolites in extracellular vesicles. *Nucleic acids research*, *47*, D516–D519. https://doi.org/10.1093/nar/gky1029

Perez-Riverol, Y., Csordas, A., Bai, J., Bernal-Llinares, M., Hewapathirana, S., Kundu, D. J., Inuganti, A., Griss, J., Mayer, G., Eisenacher, M., Pérez, E., Uszkoreit, J., Pfeuffer, J., Sachsenberg, T., Yilmaz, S., Tiwary, S., Cox, J., Audain, E., Walzer, M., … Vizcaíno, J. A. (2019). The PRIDE database and related tools and resources in 2019: Improving support for quantification data. *Nucleic acids research*, *47*, D442–D450. https://doi.org/10.1093/nar/gky1106

Raudvere, U., Kolberg, L., Kuzmin, I., Arak, T., Adler, P., Peterson, H., & Vilo, J. (2019). g:PRofiler: A web server for functional enrichment analysis and conversions of gene lists (2019 update). *Nucleic Acids Research*, *47*, W191–W198. https://doi.org/10.1093/nar/gkz369

Reddy, A., Caler, E. V., & Andrews, N. W. (2001). Plasma membrane repair is mediated by Ca(2+)-regulated exocytosis of lysosomes. *Cell*, *106*, 157–169. https://doi.org/10.1016/s0092-8674(01)00421-4

Rink, J., Ghigo, E., Kalaidzidis, Y., & Zerial, M. (2005). Rab conversion as a mechanism of progression from early to late endosomes. *Cell*, *122*, 735–749. https://doi.org/10.1016/j.cell.2005.06.043

Rock, K. L., & Kono, H. (2008). The inflammatory response to cell death. *Annual review of pathology*, *3*, 99–126. https://doi.org/10.1146/annurev.pathmechdis.3.121806.151456

Samson, A. L., Zhang, Y., Geoghegan, N. D., Gavin, X. J., Davies, K. A., Mlodzianoski, M. J., Whitehead, L. W., Frank, D., Garnish, S. E., Fitzgibbon, C., Hempel, A., Young, S. N., Jacobsen, A. V., Cawthorne, W., Petrie, E. J., Faux, M. C., Shield-Artin, K., Lalaoui, N., Hildebrand, J. M., … Murphy, J. M. (2020). MLKL trafficking and accumulation at the plasma membrane control the kinetics and threshold for necroptosis. *Nature Communication*, *11*, 3151. https://doi.org/10.1038/s41467-020-16887-1

Savina, A., Fader, C. M., Damiani, M-A. T., & Colombo, M. - A. I. (2005). Rab11 promotes docking and fusion of multivesicular bodies in a calcium-dependent manner. *Traffic (Copenhagen, Denmark)*, *6*, 131–143. https://doi.org/10.1111/j.1600-0854.2004.00257.x

Seo, J., Lee, E. - W., Sung, H., Seong, D., Dondelinger, Y., Shin, J., Jeong, M., Lee, H. - K., Kim, J. - H., Han, S. Y., Lee, C., Seong, J. K., Vandenabeele, P., & Song, J. (2016). CHIP controls necroptosis through ubiquitylation- and lysosome-dependent degradation of RIPK3. *Nature Cell Biology*, *18*, 291–302. https://doi.org/10.1038/ncb3314

Shlomovitz, I., Erlich, Z., Arad, G., Edry-Botzer, L., Zargarian, S., Cohen, H., Manko, T., Ofir-Birin, Y., Cooks, T., Regev-Rudzki, N., & Gerlic, M. (2021). Proteomic analysis of necroptotic extracellular vesicles. *Cell death & disease*, *12*, 1059. https://doi.org/10.1038/s41419-021-04317-z

Søgaard, M., Tani, K., Ye, R. R., Geromanos, S., Tempst, P., Kirchhausen, T., Rothman, J. E., & Söllner, T. (1994). A rab protein is required for the assembly of SNARE complexes in the docking of transport vesicles. *Cell*, *78*, 937–948. https://doi.org/10.1016/0092-8674(94)90270-4

Su, L., Quade, B., Wang, H., Sun, L., Wang, X., & Rizo, J. (2014). A plug release mechanism for membrane permeation by MLKL. *Structure (London, England)*, *22*, 1489–1500. https://doi.org/10.1016/j.str.2014.07.014

Sun, X., Yin, J., Starovasnik, M. A., Fairbrother, W. J., & Dixit, V. M. (2002). Identification of a novel homotypic interaction motif required for the phosphorylation of receptor-interacting protein (RIP) by RIP3. *Journal of Biological Chemistry*, *277*, 9505–9511. https://doi.org/10.1074/jbc.M109488200

Tanzer, M. C., Frauenstein, A., Stafford, C. A., Phulphagar, K., Mann, M., & Meissner, F. (2020). Quantitative and dynamic catalogs of proteins released during apoptotic and necroptotic cell death. *Cell reports*, *30*, 1260–1270.e5. https://doi.org/10.1016/j.celrep.2019.12.079

Veerman, R. E., Teeuwen, L., Czarnewski, P., Güclüer Akpinar, G., Sandberg, A., Cao, X., Pernemalm, M., Orre, L. M., Gabrielsson, S., & Eldh, M. (2021). Molecular evaluation of five different isolation methods for extracellular vesicles reveals different clinical applicability and subcellular origin. *Journal of Extracellular Vesicles*, *10*, e12128. https://doi.org/10.1002/jev2.12128

Walbrecq, G., Margue, C., Behrmann, I., & Kreis, S. (2020). Distinct cargos of small extracellular vesicles derived from hypoxic cells and their effect on cancer cells. *International Journal of Molecular Sciences*, *21*, 5071. https://doi.org/10.3390/ijms21145071

Wang, Q., Wang, P., Zhang, L., Tessema, M., Bai, L., Xu, X., Li, Q., Zheng, X., Saxton, B., Chen, W., Willink, R., Li, Z., Zhang, L., Belinsky, S. A., Wang, X., Zhou, B., & Lin, Y. (2020). Epigenetic regulation of RIP3 suppresses necroptosis and increases resistance to chemotherapy in nonsmall cell lung cancer. *Translational oncology*, *13*, 372–382. https://doi.org/10.1016/j.tranon.2019.11.011

Willoughby, P. M., Allen, M., Yu, J., Korytnikov, R., Chen, T., Liu, Y., So, I., Wan, H., Macpherson, N., Mitchell, J. A., Fernandez-Gonzalez, R., & Bruce, A. E. (2021). The recycling endosome protein Rab25 coordinates collective cell movements in the zebrafish surface epithelium. *Elife*, *10*, e66060. https://doi.org/10.7554/eLife.66060

Wu, J., Huang, Z., Ren, J., Zhang, Z., He, P., Li, Y., Ma, J., Chen, W., Zhang, Y., Zhou, X., Yang, Z., Wu, S. - Q., Chen, L., & Han, J. (2013). Mlkl knockout mice demonstrate the indispensable role of Mlkl in necroptosis. *Cell Research*, *23*, 994–1006. https://doi.org/10.1038/cr.2013.91

Yoon, S., Kovalenko, A., Bogdanov, K., & Wallach, D. (2017). MLKL, the protein that mediates necroptosis, also regulates endosomal trafficking and extracellular vesicle generation. *Immunity*, *47*, 51–65.e57. https://doi.org/10.1016/j.immuni.2017.06.001

Yu, F., Haynes, S. E., Teo, G. C., Avtonomov, D. M., Polasky, D. A., & Nesvizhskii, A. I. (2020). Fast quantitative analysis of timsTOF PASEF data with MSFragger and IonQuant. *Molecular & Cellular Proteomics*, *19*, 1575–1585. https://doi.org/10.1074/mcp.TIR120.002048

Zargarian, S., Shlomovitz, I., Erlich, Z., Hourizadeh, A., Ofir-Birin, Y., Croker, B. A., Regev-Rudzki, N., Edry-Botzer, L., & Gerlic, M. (2017). Phosphatidylserine externalization, "necroptotic bodies" release, and phagocytosis during necroptosis. *PLoS Biology*, *15*, e2002711. https://doi.org/10.1371/journal.pbio.2002711

Zhang, D. - W., Shao, J., Lin, J., Zhang, N., Lu, B. - J., Lin, S. - C., Dong, M.-Q., & Han, J. (2009). RIP3, an energy metabolism regulator that switches TNF-induced cell death from apoptosis to necrosis. *Science*, *325*, 332–336. https://doi.org/10.1126/science.1172308

Zulkefli, K. L., Houghton, F. J., Gosavi, P., & Gleeson, P. A. (2019). A role for Rab11 in the homeostasis of the endosome-lysosomal pathway. *Experimental Cell Research*, *380*, 55–68. https://doi.org/10.1016/j.yexcr.2019.04.010

SUPPORTING INFORMATION

Additional supporting information can be found online in the Supporting Information section at the end of this article.

How to cite this article: Gupta, K., Brown, K. A., Hsieh, M. L., Hoover, B. M., Wang, J., Khoury, M. K., Pilli, V. S. S., Beyer, R. S. H., Voruganti, N. R., Chaudhary, S., Roberts, D. S., Murphy, R. M., Hong, S., Ge, Y., & Liu, B. (2022). Necroptosis is associated with Rab27-independent expulsion of extracellular vesicles containing RIPK3 and MLKL. *Journal of Extracellular Vesicles*, *11,* e12261. https://doi.org/10.1002/jev2.12261